The Astrophysical Journal, 607:346–360, 2004 May 20

THE MID-INFRARED LABORATORY SPECTRA OF NAPHTHALENE ($C_{10}H_8$) IN SOLID H_2O

S. A. Sandford,[1,2] M. P. Bernstein,[1,3] and L. J. Allamandola[1]

Received 2003 September 29; accepted 2004 February 6

ABSTRACT

Polycyclic aromatic hydrocarbons (PAHs) are common throughout the universe. Gas-phase PAHs are easily detected in radiation-rich environments by the characteristic infrared (IR) *emission* bands they produce when they are excited by higher energy radiation. In contrast, in dense interstellar clouds, where the PAHs could be present as unexcited gas-phase molecules or dust grains or frozen into ice mantles, they are expected to be seen in *absorption*. We present full mid-IR spectra of the PAH naphthalene ($C_{10}H_8$) in several media to facilitate searches for PAHs in absorption in dense clouds. The positions, widths, and strengths of the absorption bands of naphthalene are significantly altered from the gas phase when it is placed in a matrix, with the extent of the alteration depending on the nature of the matrix interaction. The infrared features of gas-phase naphthalene show P, Q, and R branches characteristic of rovibrational transitions, while naphthalene in condensed forms does not. When condensed in a relatively inert matrix (e.g., Ar or N_2), the IR features produced by naphthalene are narrow (generally FWHM < 2 cm^{-1}) and may show multiple components associated with different matrix sites. In more interactive matrices (e.g., pure naphthalene and H_2O), the bands become considerably broader (factors of 3–10), show small band position shifts (0–10 cm^{-1} in either direction), and show variable changes in relative band strengths (typically factors of 1–3). There is little systematic increase or decrease in the band strengths (perhaps none). In H_2O-rich ices, naphthalene bands are relatively insensitive to concentration and temperature, with the exception that all the bands show dramatic changes as the ices are warmed through the temperature range in which amorphous H_2O ice converts to its cubic and hexagonal crystalline forms. Given the small observed band shifts ($<$10 cm^{-1}; $<$0.04 μm at 6 μm), the current database of spectra from Ar matrix–isolated PAHs should be useful for the search for PAHs in dense clouds on the basis of observed absorption band positions. Furthermore, these data permit determination of column densities to better than a factor of 3 for PAHs in dense clouds. Column density determination of detected aromatics to better than a factor of 3 will, however, require good knowledge about the nature of the matrix in which the PAH is embedded and laboratory studies of relevant samples.

Subject headings: astrochemistry — ISM: lines and bands — ISM: molecules — line: identification — molecular data

1. INTRODUCTION

Polycyclic aromatic hydrocarbons (PAHs) and related aromatic materials are thought to be present in virtually all phases of the interstellar medium (ISM) (Allamandola, Hudgins, & Sandford 1999). Interstellar PAHs have been principally detected in radiation-rich photodissociation regions, where they are present as a mixed population of gas-phase neutral and ionized molecules. Under these conditions the PAHs are excited by UV and visible light and cool through the emission of a cascade of infrared (IR) photons whose frequencies are defined by their characteristic vibrational modes. This gives rise to the well-known emission spectra with prominent features at 3050, 1610, 1300, 1160, and 890 cm^{-1} (3.28, 6.2, 7.6, 8.6, and 11.2 μm) (Allamandola, Tielens, & Barker 1989; Peeters et al. 2002).

Despite the common association of PAHs with interstellar/circumstellar infrared emission features, not all PAHs are in environments where they emit IR photons. For example, gas-phase PAHs in dense interstellar clouds will be largely screened from exciting radiation. In addition, since dense molecular clouds are extremely cold ($T < 50$ K), most PAHs in these environments should be efficiently condensed onto dust grains, either as "pure" solids or as "guest molecules" in icy grain mantles, much as is the case for most other interstellar molecules (Sandford & Allamandola 1993). Whether such PAHs are present as a cold molecular gas, as solid grains, or in mixed-molecular ice mantles, their detection requires a search for their characteristic bands in *absorption*.

There are several lines of evidence that PAHs exist in dense molecular clouds. First, it is known that aromatics in primitive meteorites and interplanetary dust particles contain deuterium enrichments that are best explained by an interstellar dense cloud chemical heritage (Sandford 2002). In addition, weak absorption features attributed to PAHs have been observed in the IR spectra of a few objects embedded in dense clouds. These include a band near 3030 cm^{-1} (3.3 μm) on the shoulder of the much stronger 3.0 μm H_2O ice feature (Smith, Sellgren, & Tokunaga 1989; Sellgren et al. 1995; Brooke, Sellgren, & Geballe 1999) and bands near 1600 cm^{-1} (6.2 μm) (Chiar et al. 2000) and 890 cm^{-1} (11.2 μm) (Bregman, Hayward, & Sloan 2000).

It has been difficult to interpret these absorption features, because of both the low spectral contrast of the bands and a lack of relevant laboratory spectra. There is a growing database of laboratory IR absorption spectra of both neutral and ionized PAHs in inert gas matrices (see, e.g., Hudgins & Allamandola 1995a, 1995b; Szczepanski, Wehlburg, & Vala 1995; Hudgins & Sandford 1998a, 1998b, 1998c and references therein),[4] but

---

[1] NASA Ames Research Center, MS 245-6, Moffett Field, CA 94035.

[2] Corresponding author; scott.sandford@nasa.gov.

[3] SETI Institute, 2035 Landings Drive, Mountain View, CA 94043.

[4] See also http://www.astrochem.org/pahdata.

these data have been taken to address the interpretation of the IR *emission* bands of interstellar *gas-phase* PAHs. However, the PAHs in dense clouds are expected to be condensed onto dust grains, largely as neutrals. Under these conditions, the PAHs will be interacting with each other and with other molecules causing changes in their IR spectral properties (band peak positions, widths, profiles, and strengths). Interpreting the IR spectra of PAHs in interstellar dense clouds will require laboratory absorption spectra of PAHs taken under realistic dense cloud conditions.

Lines of sight that probe dense molecular clouds show ices that are always dominated by solid H_2O (Sandford 1996; Ehrenfreund & Charnley 2000). Thus, for PAHs in dense clouds, the most important molecular interaction to consider is that between PAHs and H_2O. H_2O is a relatively polar molecule and can interact quite strongly with other molecules in the solid state (see, e.g., Sandford et al. 1988; Ehrenfreund et al. 1998; Dartois et al. 1999; Gerakines et al. 1999). However, while considerable work has been done on the radiation chemistry of PAHs in H_2O-rich ices (see § 3.4), little work has been done on their infrared spectral properties.

Here we present a series of laboratory IR spectra of the two-ring PAH naphthalene ($C_{10}H_8$) frozen in H_2O ice, at various concentrations and temperatures. The experimental techniques used for this work are summarized in § 2. In § 3 we examine the spectral effects of matrix type, naphthalene concentration, ice temperature, and ice photolysis on the IR spectrum of the H_2O—naphthalene system. The astrophysical implications of these laboratory results are briefly described in § 4. Data from a number of other PAHs in H_2O-rich matrices will be discussed in a future paper.

2. EXPERIMENTAL TECHNIQUES

The $H_2O—C_{10}H_8$ samples studied in this paper were vapor deposited as submicron-thick films on a CsI window. The window was held at ∼15 K and was suspended in an evacuated sample chamber at a pressure of $\sim 10^{-8}$ torr. Detailed descriptions of the deposition process and apparatus can be found elsewhere (Bernstein et al. 1995; Hudgins & Allamandola 1995a).[5]

Naphthalene has the highest vapor pressure of any PAH (∼105 mtorr at room temperature) and can be premixed with the H_2O in the vapor phase. Gas mixtures having $H_2O/C_{10}H_8 =$ 5, 10, 25, and 50, with the ratios known to better than 5%, were prepared at room temperature in glass bulbs using a glass manifold with a background pressure of $\sim 1 \times 10^{-5}$ mbar. Since the pressure in the sample bulbs fell between 2 and 20 mbar, depending on the sample, the contaminant levels associated with the mixing process are negligible compared with the impurities of our starting materials (see below).

The $H_2O—C_{10}H_8$ sample gases were vapor deposited onto the 15 K CsI substrate at a rate that produced an ∼0.1 μm thick ice layer after a few minutes of deposition. Some fractionation between the H_2O and $C_{10}H_8$ occurs early on during deposition, the mixture being depleted in $C_{10}H_8$ during the first few minutes of deposition. This effect was minimized by flowing the gas mixture onto a cold shield surrounding the sample head for ∼5 minutes prior to beginning deposition onto the cold sample window. An extensive set of calibration experiments in which the relative strengths of the H_2O and $C_{10}H_8$ bands were monitored during extended depositions indicated that under our experimental conditions the $H_2O/C_{10}H_8$ ratio of the final ice samples differed from the initial gas samples by a factor of 1.6 ± 0.3. Thus, the resulting ice samples had actual $H_2O/C_{10}H_8$ ratios of approximately 8, 15, 40, and 80. These true ratios are those reported in the tables and figures and are accurate to about 20%. Pure $C_{10}H_8$ samples were prepared by deposition of the vapor above pure solid naphthalene in a sample tube at 300 K that was attached to the sample head.

These concentrations where chosen to span the range of dilutions consistent with past reports of PAH absorption bands in dense clouds if one assumes the detected PAHs are uniformly mixed in the H_2O ice along the line of sight. Under these conditions, the PAHs in the ice are not all fully isolated from each other (Behringer 1958). If one assumes each $C_{10}H_8$ molecule substitutes for a single H_2O molecule in the ice, then ∼90% of the $C_{10}H_8$ in an ice with $H_2O/C_{10}H_8 = 80$ are fully isolated, with most of the rest of the $C_{10}H_8$ being present as dimers. At the opposite end of the range, in an $H_2O/C_{10}H_8 = 8$ sample, at most only 50% of the $C_{10}H_8$ will be in monomeric form, the rest being in dimers, trimers, and higher multimers. If $C_{10}H_8$ substitutes for more than one H_2O molecule in the ice lattice, these values represent lower limits on the fraction of monomeric $C_{10}H_8$. Thus, these samples span a range of concentrations in which both $H_2O—C_{10}H_8$ and $C_{10}H_8—C_{10}H_8$ interactions may play important roles.

This technique produces an ice composed of an intimate mixture of the $C_{10}H_8$ molecules in amorphous H_2O. This form is believed to be representative of H_2O-rich ices in interstellar molecular clouds (Allamandola & Sandford 1988; Jenniskens & Blake 1994; Jenniskens et al. 1995). Pure $C_{10}H_8$ and pure H_2O samples were made by depositing $C_{10}H_8$ and H_2O vapor, respectively, directly onto the cold window.

After deposition onto the CsI window, the 4000–500 cm^{-1} (2.5–20 μm) IR spectra of the samples were measured at a resolution of 0.9 cm^{-1} (the observed width of an unresolved line). Analyses of the areas of the resulting IR absorption bands of both the H_2O and $C_{10}H_8$ verified that our sample ice layers had thicknesses of a few tenths of a micron. Additional spectra were subsequently measured after the samples had been warmed to temperatures of 25, 50, 75, 100, 125, 150, and 175 K. Samples were warmed at a rate of ∼2 K $minute^{-1}$ between the temperature steps and were allowed to equilibrate for 5 minutes at each temperature before spectra were taken.

The H_2O in these experiments was purified via a Millipore Milli-Q water system to 18.2 MΩ and freeze/pump/thawed 3 times to remove dissolved gases prior to use. Naphthalene (99+%) was purchased from the Aldrich Chemical Company and was sublimed under vacuum prior to use.

3. RESULTS

The IR absorption spectrum of the two-ring PAH naphthalene has been extensively studied in the gas phase, in inert matrices, in various solvents, in KBr matrices, and in pure form. However, until now its spectrum in H_2O has remained largely unexplored. In the following section we report and compare the spectral properties (band positions, widths, profiles, and strengths) of $C_{10}H_8$ as a function of matrix composition, concentration, temperature, and radiation history.

3.1. *The IR Spectra of Naphthalene* ($C_{10}H_8$) *in Different Matrices*

Figure 1 shows a comparison between the 4000–500 cm^{-1} (2.5–20 μm) infrared spectra of $C_{10}H_8$ in the gas phase (Cané et al. 1996), isolated in an argon matrix ($Ar/C_{10}H_8 > 1000$)

---

[5] See also http://www.astrochemistry.org.

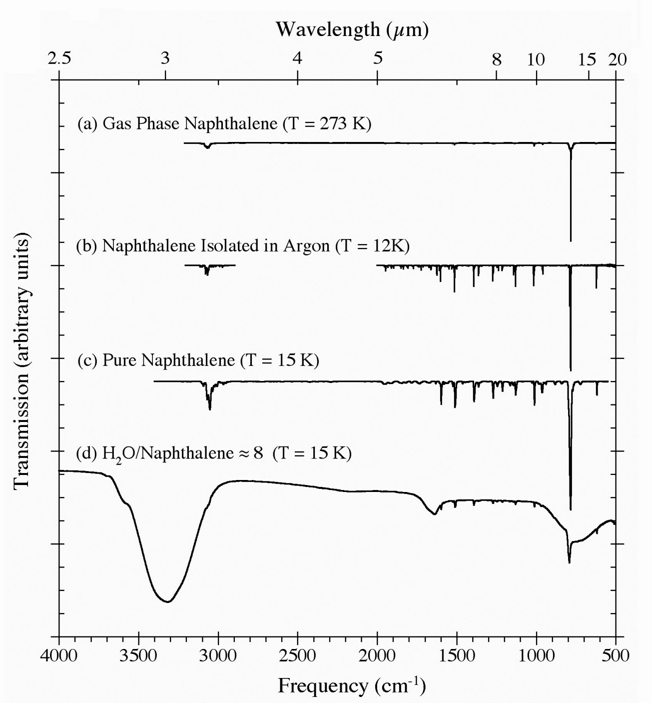

FIG. 1.—The 4000–500 cm^{-1} (2.5–20 μm) IR spectra of $C_{10}H_8$ in (*a*) the gas phase at 273 K (from Cané et al. 1996), (*b*) an argon matrix at 12 K ($Ar/C_{10}H_8 > 1000$; from Hudgins & Sandford 1998a), (*c*) in pure form at 15 K, and (*d*) in an H_2O matrix ($H_2O/C_{10}H_8 \approx 8$) at 15 K. The pure $C_{10}H_8$ spectrum was obtained by directly vacuum depositing $C_{10}H_8$ vapor onto a CsI window. Note how the strong 3300 cm^{-1} (3.0 μm) O—H stretching band of H_2O reduces the spectral contrast of the aromatic C—H stretching bands between 3150 and 2900 cm^{-1} (3.18–3.45 μm).

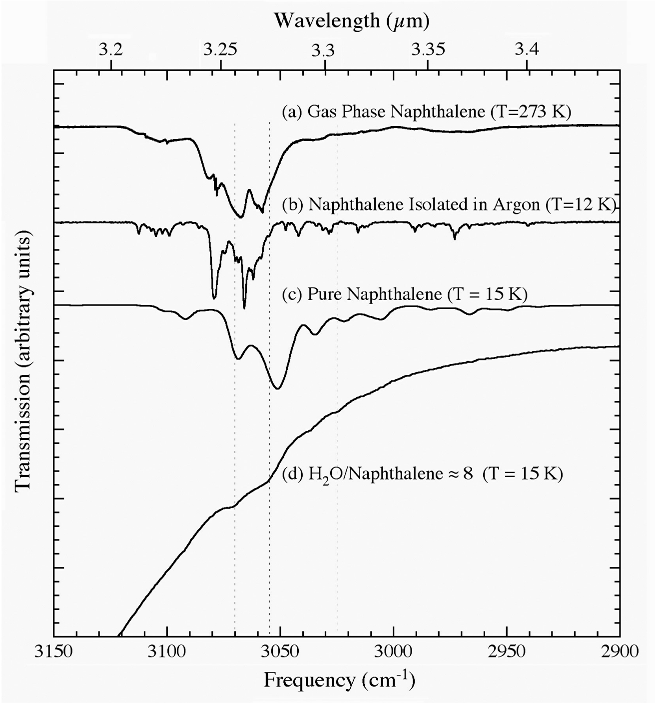

FIG. 2.—The 3150–2900 cm^{-1} (3.17–3.45 μm) IR spectra of $C_{10}H_8$ (*a*) in the gas phase at 273 K (from Cané et al. 1996), (*b*) in an argon matrix at 12 K ($Ar/C_{10}H_8 > 1000$; from Hudgins & Sandford 1998a), (*c*) in pure form at 15 K, and (*d*) in an H_2O matrix ($H_2O/C_{10}H_8 \approx 8$) at 15 K. The characteristic profiles of the *P*, *Q*, and *R* branches of the gas-phase $C_{10}H_8$ are not obvious because of extensive overlapping of multiple C—H stretching modes.

(Hudgins, Sandford, & Allamandola 1994), in pure solid form, and in an $H_2O/C_{10}H_8 \approx 8$ ice. Expansions of these data in the 3150–2900 cm^{-1} (3.17–3.45 μm) and 1300–1100 cm^{-1} (7.7–9.1 μm) ranges are shown in Figures 2 and 3, respectively. The gas-phase $C_{10}H_8$ molecules produce the classical *P*, *Q*, and *R* branch envelopes associated with the rotational transitions of isolated molecules (the individual rotation lines are unresolved). As with the gas phase, $C_{10}H_8$ molecules in Ar are isolated from one another and the resulting absorption bands are sharp. In the pure $C_{10}H_8$ sample the molecules are not isolated, but instead interact with each other. This results in significant broadening and blending of many of the bands, as well as minor shifts in peak positions (typically less than 10 cm^{-1}). $C_{10}H_8$—$C_{10}H_8$ interactions also result in changes in the relative strengths of the bands (Witteborn et al. 1989). In the $H_2O/C_{10}H_8 \approx 8$ sample all the naphthalene molecules interact with multiple H_2O molecules and many interact with one or more adjacent $C_{10}H_8$ molecules. These interactions result in band broadening, blending, and shifting similar to, but not identical with, those in the pure $C_{10}H_8$ sample.

Table 1 contains a summary of the band positions, widths, and relative strengths of $C_{10}H_8$ in $H_2O/C_{10}H_8 \approx 8$, 15, and 40 samples, pure $C_{10}H_8$, and $C_{10}H_8$ isolated in argon. Values are not provided for $H_2O/C_{10}H_8 \approx 80$ because most of the bands in this mixture are too weak to be properly quantified. Relative band areas have been normalized to the $C_{10}H_8$ band near 1390 cm^{-1} (7.19 μm). The stronger out-of-plane bending mode band near 790 cm^{-1} (12.7 μm) was not used for normalization because it falls on the H_2O libration feature and it is often difficult to uniquely define its baseline. It is apparent from Table 1 and Figures 1–3 that the spectrum of $C_{10}H_8$ in

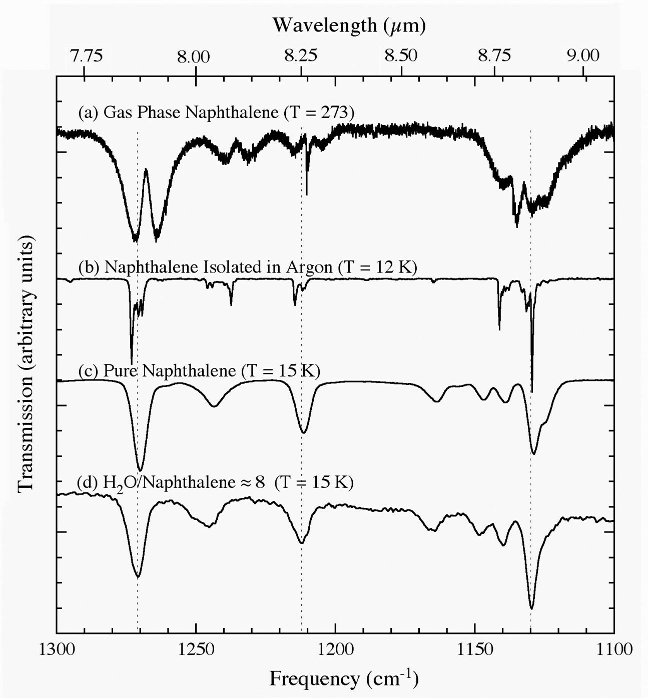

FIG. 3.—The 1300–1100 cm^{-1} (7.7–9.1 μm) IR spectra of $C_{10}H_8$ (*a*) in the gas phase at 273 K (from Cané et al. 1996), (*b*) in an argon matrix at 12 K ($Ar/C_{10}H_8 > 1000$; from Hudgins & Sandford 1998a), (*c*) in pure form at 15 K, and (*d*) in an H_2O matrix ($H_2O/C_{10}H_8 \approx 8$) at 15 K. Solid-state interactions result in bands broadening, blending, shifting, and, in some cases, changing their relative strengths.

TABLE 1

Infrared Band Positions, Widths, and Strengths of Naphthalene in Different Matrices at 15 K

Pure Naphthalene		H_2O/Naphthalene = 8		H_2O/Naphthalene = 15		H_2O/Naphthalene = 40		Naphthalene in Argon[a]	
Band Position (FWHM)[b] (cm^{-1})	Relative Intensity[c]	Band Position (FWHM)[b] (cm^{-1})	Relative Intensity[c]	Band Position (FWHM)[b] (cm^{-1})	Relative Intensity[c]	Band Position (FWHM)[b] (cm^{-1})	Relative Intensity[c,d]	Band Position (FWHM)[b] (cm^{-1})	Relative Intensity[c]
618.0 (3.0)	0.34	617.8 (2.7)	0.50	618.0 (2.8)	0.58	617.8 (~3)	0.28	621.2, 619.3 (0.5, 0.9)	0.58
783.4* (10.0)	14.8	791.5 (14.1)	14.6	791.2 (16.1)	13.4	791.3 (15.5)	12.3	788.2, 783.4 (0.9, 0.9)	15.9
937.8 (2.4)	0.04	939.2 (3.4)	0.06	939.7 (~3)	...			939? (?)	...
962.2 (8.4)	0.58	968.8 (8.4)	0.38	968.3 (7.7)	0.34	~969? (?)	...	957.6* (1.6)	0.55
1010.6* (3.6)	0.75	1010.4 (4.3)	0.62	1010.7 (4.3)	0.67	1011.1 (4.0)	0.35	1016.4, 1012.4 (0.7, 1.5)	1.13
1025.2 (4.3)	0.05	1024.8 (3.3)	0.03	1024.9 (~4)	0.04	~1024 (?)	<0.5		
1128.9* (7.4)	0.64	1129.6 (4.8)	0.57	1129.9 (4.4)	0.54	1130.1 (3.4)	0.31	1129.1* (0.5)	0.81
1139.1 (4.2)	0.10	1139.9 (5.2)	0.10	1139.8 (4.9)	0.15	1139.7 (~3)	0.05	1140.9* (0.6)	0.32
1146.8 (5.0)	0.10	1148.4 (5.3)	0.09						
1163.5 (6.6)	0.16	1165.3 (6.2)	0.14	1164.9 (~6)	0.19	1163 (?)	...	1164.5 (1.2)	0.03
1211.4 (5.8)	0.42	1212.0 (6.8)	0.27	1212.2 (6.6)	0.32	1211.4 (~4)	0.16	1214.2* (1.1)	0.30
1243.6 (8.0)	0.30	1246.0 (10.7)	0.29	1245.8 (~9)	0.31			1237.1* (0.8)	0.35
1270.0 (5.4)	0.71	1271.0 (6.5)	0.58	1270.9 (6.3)	0.60	1271.3 (6.0)	0.41	1272.8* (1.1)	1.11
1361.9 (4.6)	0.19	1363.4*, 1354.9 (5.3, ~6)	0.17	1364.1 (5.5)	0.16	1362.3? (?)	...	1361.6 (0.7)	0.28
1390.2 (6.4)	*1.00*	1391.4 (5.6)	*1.00*	1391.3 (5.5)	*1.00*	1391.8 (4.7)	*1.00*	1391.8* (0.8)	*1.00*
1507.5, 1510.5 (7.4)	1.41	1510.1* (8.0)	1.59	1510.7, 1506.9 (8.0)	1.57	1510.9 (7.2)	1.09	1513.0*, 1498.9 (0.7, 1.7)	1.21
1462.1 (5.0)	0.08								
1523.7 (4.4)	0.15	1523.1 (5.2)	0.16	1523.0 (6.1)	0.15	1523.3 (1.2)	0.03	1525.5 (1.6)	0.02
								1547.7 (1.5)	...
1578.6 (3.5)	0.04	1578.3 (3.0)	0.05	1578? (?)	...				
1596.7 (4.2)	0.65	1596.7 (4.1)	0.68	1597.2 (4.3)	0.64	1597.8 (4.3)	0.39	1604.4 (1.2)	0.92
1671.9? (21.6)	0.26							1672.1 (1.5)	...
1733.6 (21.2)	0.39							1722.4 (1.5)	0.33
1782.2 (14.6)	0.16							1738.4* (1.5)	...
								1771.1* (1.4)	...
1819.5 (16.9)	...	~1796 (~17)	0.13					1806.3* (1.7)	...
1843.9 (25.5)	...								
1875–1795	0.52	~1830 (~15)	0.09					1834.6* (0.8)	...
		1861.9 (19.9)	0.19	~1860 (~17)	0.18			1848.8 (1.7)	...
				~1920 (~22)	0.14			1895.7* (1.4)	...

TABLE 1—*Continued*

Pure Naphthalene		H_2O/Naphthalene = 8		H_2O/Naphthalene = 15		H_2O/Naphthalene = 40		Naphthalene in Argon[a]	
Band Position (FWHM)[b] (cm^{-1})	Relative Intensity[c]	Band Position (FWHM)[b] (cm^{-1})	Relative Intensity[c]	Band Position (FWHM)[b] (cm^{-1})	Relative Intensity[c]	Band Position (FWHM)[b] (cm^{-1})	Relative Intensity[c,d]	Band Position (FWHM)[b] (cm^{-1})	Relative Intensity[c]
1914.0 (27.5)	...							1909.8* (1.3)	...
1953.1 (27.1)	...	1923.4 (18.6)	0.17					1931.5* (1.8)	...
1975–1890	0.91	1966.3 (17.5)	0.19	~1961 (~25)	0.27	~1960 (?)	~0.2	1945.1 (1.7)	0.34
3051.3* (13.1)	...	~3071 (~5)	...	~3071(~5)	...	~3071(?)	...	3065.0*(2.7)	...
3114–2995[e]	6.12[e]	~3055 (~12)	...	~3055 (~10)	...	~3060? (?)	...	3078.2* (4.1)	...
		3080–3040	(6)[f]	3080–3040	(6)[f]	3080–3050	(6)[f]	3117–2934[e]	10.35[e]
								3087–3048[e]	7.14[e]

[a] Ar matrix data are taken from Hudgins & Sandford 1998a.

[b] An asterisk signifies that the value is the position of the strongest band(s) or an associated group of bands. Only the strongest of the C—H stretching bands are listed.

[c] Normalized to the band near 1390 cm^{-1}. The relative band strengths for the $H_2O—C_{10}H_8$ samples can be converted into absolute strengths by multiplying them by a factor of 8.1×10^{-19} cm $molecule^{-1}$ (see § 3.6).

[d] Relative intensities are somewhat uncertain because of the weakness of the naphthalene bands in this mixture. The uncertainty increases with the weakness of the band.

[e] Relative band area of all the C—H stretching bands within the stated frequency range.

[f] Estimated after subtractions of a portion of the underlying 3.0 μm H_2O absorption band (see § 3.5).

solid H_2O most closely resembles that of pure solid $C_{10}H_8$, although there are small differences.

Remarkably, in spite of these effects, band position differences between $C_{10}H_8$ isolated in Ar, pure $C_{10}H_8$, and $C_{10}H_8$ in H_2O are everywhere less than 11 cm^{-1}, and usually less than 5 cm^{-1}. Some peak positions are relatively insensitive to molecular environment. For example, the bands near 618, 1130, 1140, 1165, 1212, 1271, 1363, and 1392 cm^{-1} (16.2, 8.850, 8.772, 8.584, 8.251, 7.868, 7.337, and 7.184 μm) all fall within the same 2 cm^{-1} region, independent of matrix. Larger positional shifts can be in either direction. For example, the peak positions of $C_{10}H_8$ in Ar fall to lower frequencies than $C_{10}H_8$ in H_2O for the bands near 791, 969, and 1246 cm^{-1} (12.6, 10.3, and 8.026 μm, all C—H bending modes), but at higher frequencies for those near 1011, 1510, 1523, and 1598 cm^{-1} (9.891, 6.623, 6.566, and 6.258 μm, all C—C vibrations). While the shifts in pure $C_{10}H_8$ are small (usually <2 cm^{-1}, always ≤ 6 cm^{-1}), the features in its spectrum systematically fall at the same or lower frequencies than in the spectra of the H_2O—$C_{10}H_8$ samples.

The band widths of pure $C_{10}H_8$ and $C_{10}H_8$ in H_2O are very similar to each other and both are significantly larger than seen for $C_{10}H_8$ isolated in Ar. In both cases, the degree of increased width relative to Ar-isolated $C_{10}H_8$ varies from band to band. A factor of 3 increase is the smallest seen, and increases of factors of 5–10 are common. The width of the rotational envelopes of the gas-phase $C_{10}H_8$ bands is due to the population of rotational states present in a room temperature gas (Cané et al. 1996). Only the lower rotation states would be filled in a cold (10 K) interstellar $C_{10}H_8$ gas, and the observed envelopes would be considerably (more than a factor of 2) narrower.

As with band widths, the relative band strengths of pure $C_{10}H_8$ and $C_{10}H_8$ in H_2O are similar to each other and can differ significantly from $C_{10}H_8$ isolated in Ar. Again, the differences vary from feature to feature. In Table 1 the relative band areas are all normalized to the 1390 cm^{-1} band. Past comparisons of theoretical relative band strengths for gas-phase $C_{10}H_8$ and those measured in Ar matrix isolation experiments have shown good general agreement, with most features matching to better than 30% (Hudgins & Sandford 1998*a*, 1998b, 1998c). However, the relative strengths of the bands of pure and H_2O-isolated $C_{10}H_8$ are frequently significantly different from those of Ar matrix–isolated $C_{10}H_8$, and, to a lesser extent, differ from each other. The range of differences between the various absorptions of $C_{10}H_8$ in H_2O and pure $C_{10}H_8$ (0.7–1.7) is significantly smaller than that between $C_{10}H_8$ in H_2O and $C_{10}H_8$ isolated in Ar (0.3–5). There is a tendency for the features that show the smallest positional shifts to show smaller relative band strength variations, but there are clear exceptions.

The variability in the relative band strengths compared to Ar-isolation data and theoretical calculations is clear evidence that different vibrational modes interact with adjacent $C_{10}H_8$ or H_2O molecules in different ways, with each interaction yielding its unique enhancement or suppression of the feature's *intrinsic* strength. While the differences in relative band strengths due to the different matrices can serve as a diagnostic feature for identification of the matrix condition of the $C_{10}H_8$, they do not, in and of themselves, define whether an individual feature's strength increases, decreases, or stays the same relative to its gas-phase value. As a result, use of the predicted *absolute* band strengths of gas-phase PAHs in conjunction with the *relative* band areas of the measured spectra of pure $C_{10}H_8$ or H_2O—$C_{10}H_8$ mixtures provided in Table 1 will likely result in derived column densities with systematic offsets from their true values. The size and direction of the offset will depend on which calculated band strength is selected for normalization. At least one absolute band strength is needed to resolve this issue. A discussion of the factor needed to convert the *relative* band strengths in Table 1 into *absolute* band strengths is provided in § 3.6.

While generally similar with regard to band positions, widths, and relative strengths, there are some distinct differences between the spectra of pure $C_{10}H_8$ and $C_{10}H_8$ in H_2O. First, the presence of the very strong 3300 cm^{-1} (3.0 μm) O—H stretching band of H_2O results in a dramatic decrease in the spectral contrast of the naphthalene C—H stretching modes between 3150 and 2900 cm^{-1} (3.18–3.45 μm). This issue is addressed separately in § 3.5. Second, the widths and positions of overtone/combination bands in the 2000–1750 cm^{-1} (5.0–5.7 μm) region show greater differences than the fundamental modes. This is also true of the relative band strengths, with the pure $C_{10}H_8$ showing greater overall absorption strength in this region.

The large spectral effect of the H_2O matrix interaction relative to isolated $C_{10}H_8$ is not particularly surprising given that many other molecules show similar effects when frozen in H_2O ices. The H_2O matrix effects for other guest molecules are typically concentration- and temperature-dependent (see, e.g., Sandford et al. 1988; Sandford & Allamandola 1990; Ehrenfreund et al. 1998). These parameters are examined in the following two sections.

3.2. *The Effects of Concentration on the Spectra of* H_2O—$C_{10}H_8$ *Ices*

Figures 4 and 5 compare the 1800–1000 cm^{-1} (5.56–10.0 μm) and 1000–500 cm^{-1} (10–20 μm) IR spectra, respectively, of 15 K samples of pure $C_{10}H_8$ and pure H_2O with mixed ices having $H_2O/C_{10}H_8$ ratios of approximately 8, 15, 40, and 80. These values are likely to span the detectable concentrations of neutral PAHs in interstellar ices under most conditions. The C—H stretching bands falling between 3150 and 2900 cm^{-1} (3.18–3.45 μm) are addressed in § 3.5.

Pure $C_{10}H_8$ and H_2O—$C_{10}H_8$ mixes produce bands that generally have similar relative strengths and widths. Band positions are also similar, but modest matrix-induced shifts are seen. Other than the expected decrease in strength of the $C_{10}H_8$ bands relative to the H_2O bands, very little changes as the concentration of $C_{10}H_8$ is decreased in the H_2O matrix.

The properties of the $C_{10}H_8$ absorption bands in H_2O—$C_{10}H_8$ ices as a function of $C_{10}H_8$ concentration are summarized in Table 1. The relative band strengths have been normalized to the strength of the band near 1390 cm^{-1} (7.19 μm). Again, values are not provided for H_2O—$C_{10}H_8 \approx 80$ because most of the bands in this mixture are too weak to be properly quantified.

Peak positions remain essentially the same across the entire range $H_2O/C_{10}H_8 \approx 8$–40. Variations in position are less than 2 cm^{-1} and show no systematic trends with concentration, suggesting that the majority of the observed variation is due to uncertainties in the baselines and identification of the centroids of the features. This is especially true of the very weak features produced by the $H_2O/C_{10}H_8 \approx 80$ sample, where band positions vary by up to $\sim$5 cm^{-1}. Band widths are also relatively unaffected by concentration, although there may be a weak tendency for them to narrow slightly with decreasing concentration. This would not be surprising since greater dilution will decrease the proportion of $C_{10}H_8$—$C_{10}H_8$

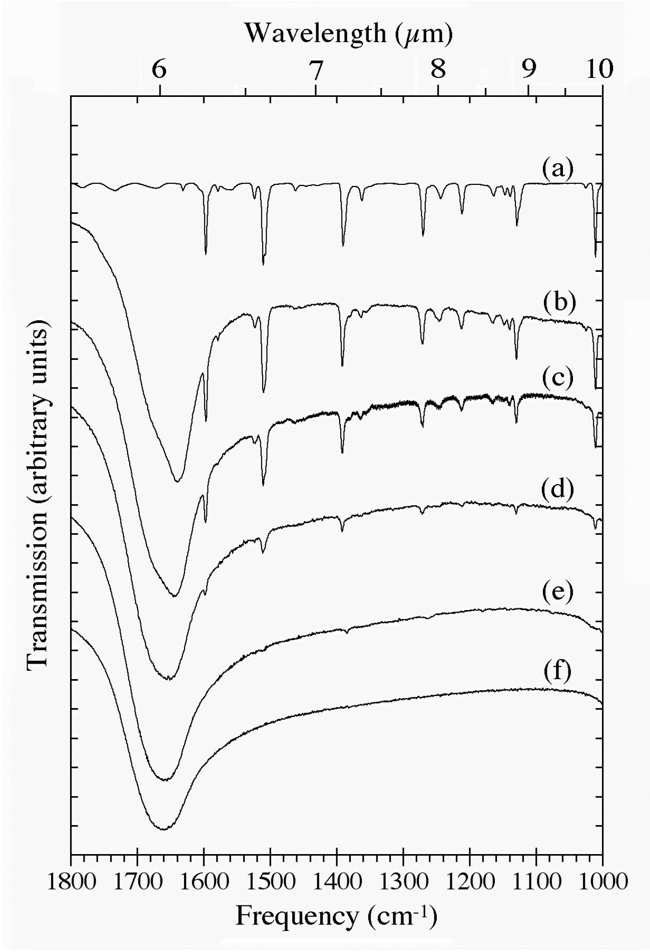

FIG. 4.—The 1800–1000 cm^{-1} (5.56–10.0 μm) IR spectra of $H_2O-C_{10}H_8$ ices as a function of $C_{10}H_8$ concentration. Naphthalene bands in this region are largely due to C—C stretching and C—H in-plane bending modes. The spectra are from (*a*) pure $C_{10}H_8$, (*b*) $H_2O/C_{10}H_8 \approx 8$, (*c*) $H_2O/C_{10}H_8 \approx 15$, (*d*) $H_2O/C_{10}H_8 \approx 40$, (*e*) $H_2O/C_{10}H_8 \approx 80$, and (*f*) pure H_2O. The very broad band centered near 1660 cm^{-1} (6.0 μm) is due to H—O—H bending modes of the H_2O. All spectra were taken from samples deposited and maintained at 15 K.

interactions and result in a somewhat smaller overall distribution of matrix sites and interactions.

It is difficult to establish how relative band strengths vary with concentration for all but the strongest $C_{10}H_8$ features because the weaker ones are difficult to detect and/or measure reliably at the lower concentrations. There are no significant differences in strengths between the $H_2O/C_{10}H_8 \approx 8$ and 15 samples. Bands strong enough to be measured in the $H_2O/C_{10}H_8 \approx 40$ sample show slightly larger strength variations but still usually lie within 30% of the values at higher concentrations. These larger variations could be due to increased isolation of the $C_{10}H_8$ in the $H_2O/C_{10}H_8 \approx 40$ sample with its corresponding decrease in the number of $C_{10}H_8-C_{10}H_8$ interactions.

In summary, when they can be measured, the positions and widths of the absorption features of $C_{10}H_8$ are quite insensitive to the concentration of $C_{10}H_8$ in the H_2O matrix. Relative band strengths show greater variation but vary by only about 30% across the concentrations that can be reliably measured.

3.3. *The Effects of Temperature on the Spectra of* $H_2O-C_{10}H_8$ *Ices*

All the $H_2O-C_{10}H_8$ samples were warmed to temperatures of 25, 50, 75, 100, 125, 150, and 175 K after deposition at 15 K. Figures 6 and 7 show the 1800–1000 cm^{-1} (5.56–10.0 μm) and 1000–500 cm^{-1} (10–20 μm) IR spectra, respectively, of an $H_2O/C_{10}H_8 \approx 15$ sample deposited at 15 K and subsequently warmed to temperatures of 25, 50, 75, 100, 125, 150, and 175 K. The spectral bands of $C_{10}H_8$ do not change substantially as the sample is warmed up to 125 K, but major changes occur as the sample is warmed to higher temperatures. The same temperature-dependent behaviors were seen for all the $C_{10}H_8$ concentrations examined.

For all concentrations, the strengths and profiles of the $C_{10}H_8$ bands remain largely unchanged, as do most of the positions, as the samples are warmed from 15 to 125 K. Some bands show very minor systematic shifts in their position (generally ≤ 2.5 cm^{-1} in either direction) as the sample is warmed to 125 K. The largest change is for the out-of-plane bending mode near 791.2 cm^{-1}, which moves 3.2 cm^{-1} downward as the temperature rises from 15 to 125 K.

The spectrum changes radically once the temperature of the sample rises above 125 K, however. Between 125 and 150 K most of the bands change in one or more of the following ways: (1) most bands become considerably narrower, (2) many features show modest shifts in position, and (3) many features split into multiple (usually 2 or 3) components. The extent of these effects differs from band to band. Those that

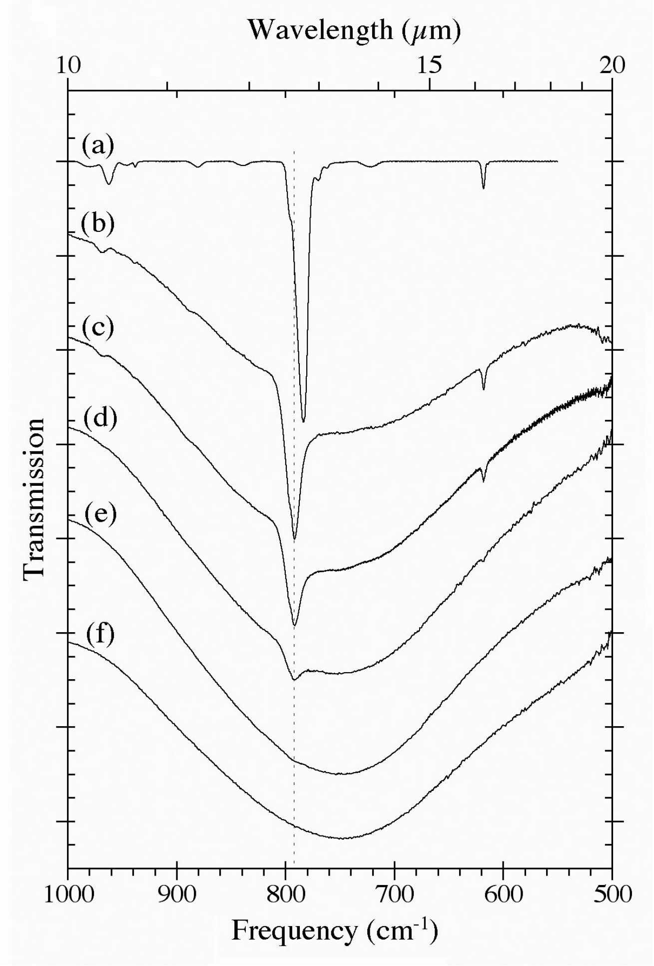

FIG. 5.—The 1000–500 cm^{-1} (10.0–20.0 μm) IR spectra of $H_2O-C_{10}H_8$ ices as a function of $C_{10}H_8$ concentration. Naphthalene bands in this region are largely due to C—H out-of-plane bending modes. The spectra are from (*a*) pure $C_{10}H_8$, (*b*) $H_2O/C_{10}H_8 \approx 8$, (*c*) $H_2O/C_{10}H_8 \approx 15$, (*d*) $H_2O/C_{10}H_8 \approx 40$, (*e*) $H_2O/C_{10}H_8 \approx 80$, and (*f*) pure H_2O. The very broad band centered near 750 cm^{-1} (13.3 μm) is due to librational modes of the H_2O. All spectra were taken from samples deposited and maintained at 15 K.

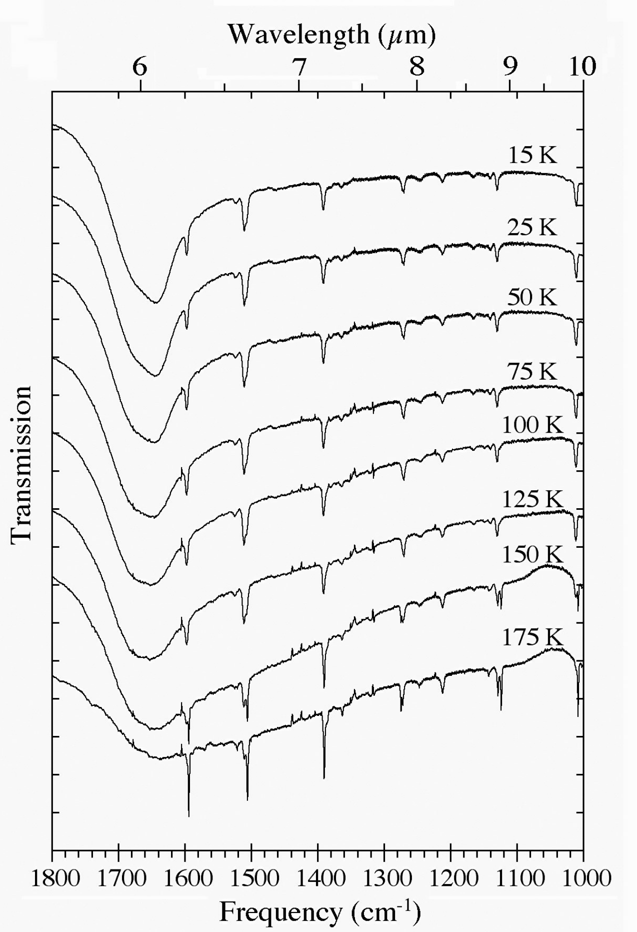

FIG. 6.—The 1800–1000 cm^{-1} (5.56–10.0 μm) spectra of an $H_2O/C_{10}H_8 \approx 15$ ice as a function of ice temperature. Spectra were taken from the same sample after it was deposited at 15 K and subsequently warmed in steps at 2 K $minute^{-1}$ to temperatures of 25, 50, 75, 100, 125, 150, and 175 K. The very broad band centered near 1660 cm^{-1} (6.0 μm) is due to H—O—H bending vibrations of the H_2O. Note the band splitting that occurs at temperatures above 125 K as the original amorphous H_2O ice matrix is transformed into its cubic phase.

are not split typically shift less than 1 cm^{-1} to either higher or lower frequency, the major exception being the band near 968 cm^{-1} that moves over 5 cm^{-1} to lower frequency between 125 and 150 K. Peaks that split generally show larger shifts in position (up to as much as 10 cm^{-1} relative to their values at 125 K), with the span of the various components typically lying between 3 and 15 cm^{-1}. The temperature-dependent changes that occur between 125 and 150 K to the positions, widths, and relative strengths of the $C_{10}H_8$ features in the $H_2O—C_{10}H_8 \approx 15$ sample are summarized in Table 2. Relative band strengths are normalized to the strength of the feature near 1390 cm^{-1} (7.19 μm).

These changes are driven by the H_2O phase transformation from amorphous to cubic ice above 125 K. Above about 150 K, some of the ice may also begin to transform to crystalline hexagonal ice (Jenniskens & Blake 1994; Jenniskens et al. 1995). The vibrational bands of $C_{10}H_8$ in amorphous H_2O ices are generally broad and featureless because of the fairly random orientations of both species. During the amorphous-to-crystalline phase transformation, the individual H_2O molecules in the ice matrix rearrange from their original "random" orientations into well-defined structures. As a result, guest molecules find themselves in a more limited range of discrete molecular sites and therefore interactions. The original broad, largely featureless bands of the guest molecule can split into multiple, narrower bands or show sharp changes in band position. This effect is well established for CO and CO_2 in H_2O ices transforming to cubic form (Sandford et al. 1988; Sandford & Allamandola 1990; Ehrenfreund et al. 1998) and in $H_2O—CH_3OH$ ices as they transform into type II clathrates (Blake et al. 1991).

Spectral changes that occur during this transition are diagnostic of the $H_2O—C_{10}H_8$ interaction and the H_2O ice structure but are of limited relevance to the ISM, where ices would sublime rapidly above 125 K (Sandford & Allamandola 1993 and references therein). It is unlikely that PAHs frozen in warm ($T > 125$ K) H_2O-rich ices are abundant in the ISM. In this regard, it should be noted that the spectra of the 150 and 175 K ices were taken from ices that were subliming. This sublimation resulted in the loss of H_2O relative to $C_{10}H_8$, so the $H_2O/C_{10}H_8$ ratios of the samples at these temperatures are likely somewhat lower than those of the original 15 K ices.

As with the peak positions, band widths do not change appreciably as the samples are warmed from 15 to 125 K. There is a tendency for many of the features to narrow very slightly over this temperature range, but the reduction is generally less than 10%. This behavior is common in the spectra of other molecules frozen in H_2O-rich matrices and is

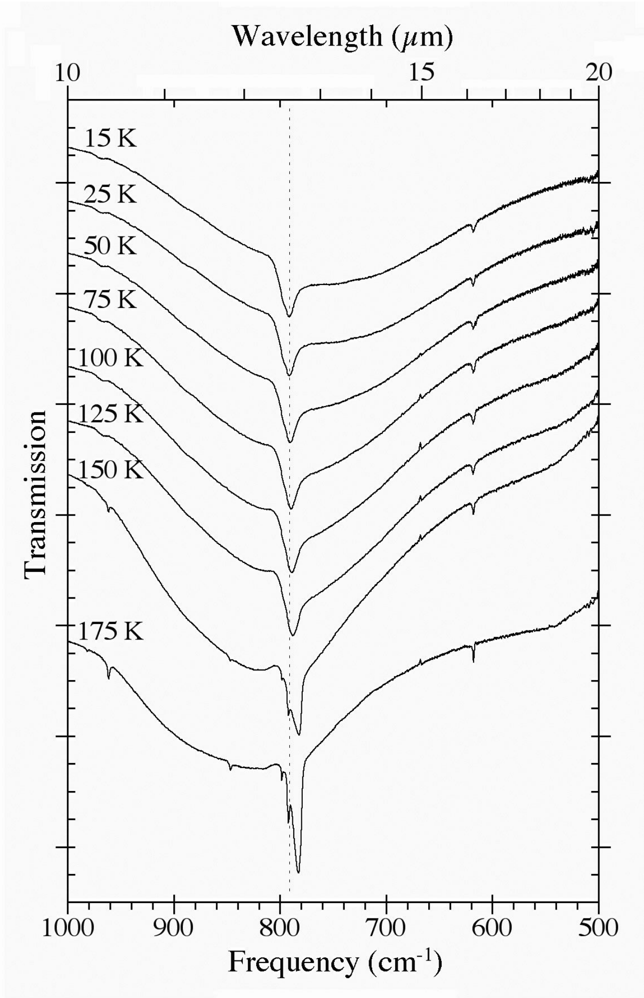

FIG. 7.—The 1000–500 cm^{-1} (10.0–20.0 μm) spectra of an $H_2O/C_{10}H_8 \approx 15$ ice as a function of ice temperature. Spectra were taken from the same sample after it was deposited at 15 K and subsequently warmed in steps at 2 K $minute^{-1}$ to temperatures of 25, 50, 75, 100, 125, 150, and 175 K. The very broad band centered near 750 cm^{-1} (13.3 μm) is due to librational modes of the H_2O. Note the band splitting that occurs at temperatures above 125 K as the original amorphous H_2O ice matrix is transformed into its cubic phase.

TABLE 2

Infrared Band Positions, Widths, and Strengths of $H_2O/C_{10}H_8 \approx 15$ before and after H_2O Crystallization

H_2O/Naphthalene = 15			
125 K		150 K	
Band Position (FWHM)[a] (cm^{-1})	Relative Intensity[b]	Band Position (FWHM)[a] (cm^{-1})	Relative Intensity[b]
618.2 (2.7)	0.52	617.8 (1.8)	0.42
788.0 (14.7)	15.8	788.0, 782.0 (13.8)	22.1
966.4 (8.0)	0.46	961.3 (1.9)	0.24
1011.2 (3.9)	0.70	1011.0, 1007.7 (4.7, 1.5)	0.64
1129.8 (4.3)	0.59	1129.0, 1123.9 (4.5, 1.8)	0.75
1139.9 (4.4)	0.10	1140.6 (~5)	0.14
1164.2 (5.2)	0.10	1164.3 (3.3)	0.06
1212.0 (5.6)	0.31	1212.0 (3.9)	0.33
1245.0 (8.3)	0.26	1245.6 (~6)	0.25
1270.4 (5.2)	0.65	1274.6, 1271.7 (~2.3, ~5)	0.66
1363.9 (5.2)	0.13	1363.6 (2.1)	0.09
1391.1 (4.5)	*1.00*	1390.3 (2.7)	*1.00*
1510.9 (8.1)	1.74	1511.0, 1505.7 (~4, 2.6)	1.33
1597.1 (4.5)	0.67	1597.3, 1593.9* (1.8)	0.67
1859.6 (~20)	0.21	1860?	. . .
1926.9 (~8)	0.12	1926?	. . .
		1923.4 (18.6)	0.17
1959.2 (~20)	0.18	1958.3 (13.1)	0.11
~3071 (~5)	. . .	~3071 (~5)	. . .
~3055 (~10)	. . .	~3055 (~12)	. . .
3080–3040	(6)[c]	3080–3040	(6)[c]

[a] An asterisk signifies that the value is the position of the strongest band(s) or an associated group of bands. Only the strongest of the C—H stretching bands are listed.

[b] Normalized to the band near 1390 cm^{-1}. The relative band strengths can be converted into absolute strengths by multiplying them by a factor of 8.1×10^{-19} cm molecule^{-1} (see § 3.6).

[c] Estimated after subtraction of a portion of the underlying 3.0 μm H_2O absorption band (see § 3.5).

associated with minor rearrangement of some of the H_2O molecules during warming, leading to a slight decrease in the range of H_2O orientations. Band widths decrease dramatically when the ice is warmed above 125 K, typically by factors of 2–4. Again, this is due to the crystallization during which H_2O molecules reorient from their wide range of original "random" orientations into well-defined structural orientations. Note that there is still significant $H_2O{-}C_{10}H_8$ and $C_{10}H_8{-}C_{10}H_8$ interaction after crystallization: the bands in 150 K samples are still 2–5 times wider than those observed when the $C_{10}H_8$ is isolated in an inert argon matrix (see Tables 1 and 2).

The relative strengths of the $C_{10}H_8$ bands are fairly insensitive to the temperature of the H_2O matrix, varying by less than 30% over the entire 15–125 K temperature range. Since the structural order of the H_2O matrix changes significantly when the H_2O ice crystallizes, it would not be surprising if individual relative band areas changed somewhat after the transformation to cubic ice. While there are larger-than-average differences in relative band areas after crystallization compared to other heating steps, the changes are still usually less than 30%. As was the case for the concentration studies, the relative band strengths of $C_{10}H_8$ in H_2O ice are generally similar to those of pure $C_{10}H_8$ and quite different from those of $C_{10}H_8$ in Ar. Again, a discussion of the factor needed to convert the *relative* band strengths in Table 2 into *absolute* strengths is provided in § 3.6.

3.4. *The Effects of Photolysis on the Spectra of* $H_2O{-}C_{10}H_8$ *Ices*

Considerable laboratory work has been carried out in recent years on the UV and proton irradiation of H_2O-rich ices containing various PAHs, including naphthalene, at concentrations in the range considered here (Bernstein et al. 1999, 2001, 2002, 2003). However, these studies concentrated on the creation of new molecular species and made only sparing use of IR spectroscopy as an analytical technique. Examination of the spectra available from the earlier Bernstein et al. studies indicates that photolysis does not produce any major changes in the positions, widths, or profiles of any of the infrared bands associated with the neutral PAHs (including naphthalene) present in the ice before and after irradiation at 15 K. However, these earlier spectra are of insufficient quality to measure subtle variations of the PAH bands and do not preclude the types of spectral changes sometimes seen for other molecules irradiated in H_2O-rich ices, i.e., band position and width changes of a few cm^{-1}. Determination of the presence or absence of such subtle radiation-induced spectral effects will be reported in a future paper.

3.5. *The* C—H *Stretching Band of Naphthalene in* H_2O*-rich Ices*

It is very difficult to measure the precise positions, widths, and especially strengths of the naphthalene C—H features in the 3150–2950 cm^{-1} (3.17–3.39 μm) region because of the underlying concave slope of the strong O—H stretching band of H_2O. The changing slope imposed by the H_2O makes it difficult to define the baselines underlying the features and suppresses their apparent strengths. Straight baselines drawn under such features will always *underestimate* the true strength of the C—H stretching bands. The result is that the spectral contrast of the aromatic C—H stretching mode bands

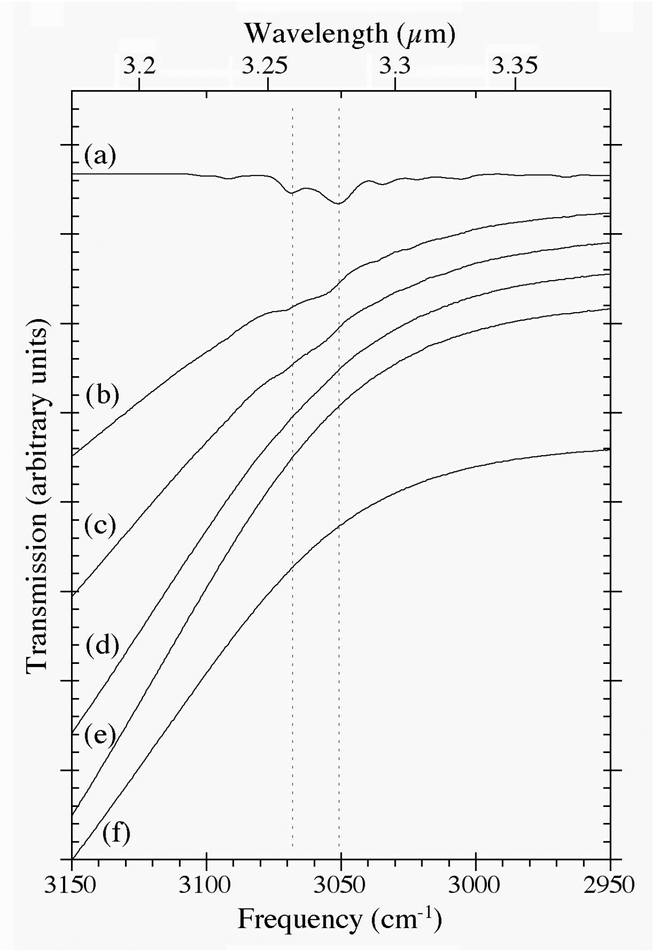

FIG. 8.—The 3150–2950 cm^{-1} (3.17–3.39 μm) IR spectra of $H_2O—C_{10}H_8$ ices as a function of $C_{10}H_8$ concentration. The spectra are from (*a*) pure $C_{10}H_8$, (*b*) $H_2O/C_{10}H_8 \approx 8$, (*c*) $H_2O/C_{10}H_8 \approx 15$, (*d*) $H_2O/C_{10}H_8 \approx 40$, (*e*) $H_2O/C_{10}H_8 \approx 80$, and (*f*) pure H_2O. The steep drop-off to higher frequencies is due to the shoulder of the very strong O—H stretching band of H_2O ice centered near 3300 cm^{-1} (3 μm). All spectra were taken from samples deposited and maintained at 15 K.

are greatly reduced when placed in an H_2O ice (see Fig. 1). Figure 8 shows the C—H stretching region for the same concentration series shown in Figure 4 and 5 and described in § 3.2. The C—H stretching features are quite subtle even at the highest concentrations examined ($H_2O/C_{10}H_8 \approx 8$ and 15). The $C_{10}H_8$ bands become virtually invisible at lower concentrations, although $C_{10}H_8$ absorption is still present.

The individual features can be partially "recovered" if the spectra of pure H_2O ices are subtracted out. However, such corrections are, at best, imperfect, since the profile of the H_2O feature is temperature dependent and is affected by the presence of other molecular species. For example, Figure 9 shows the profile of the 3.0 μm H_2O feature for pure H_2O and our various $H_2O/C_{10}H_8$ mixes. The H_2O band profile for the $H_2O/C_{10}H_8 \approx 80$ sample is very similar to that of pure H_2O. However, as the concentration of $C_{10}H_8$ increases, the band centroid shifts to higher frequencies, the low frequency shoulder rises, and a prominent feature due to dangling O—H bonds grows near 3600 cm^{-1} (2.8 μm). These profile changes make it impossible to perfectly subtract out the H_2O absorption component underlying the aromatic C—H stretching bands.

Minor subtractions of the H_2O absorption component (<25% of the 3.0 μm feature) improve the contrast of the C—H stretching features slightly, but band area integrations of the residuals yield low band strengths relative to the 1390 cm^{-1} $C_{10}H_8$ feature (values of 1.2–2.0, compared to a value of 6.12 for pure $C_{10}H_8$). Progressively larger H_2O subtractions yield increasing band contrast and larger relative band strengths. As an example, the lower trace in Figure 9 shows the spectrum that results if 75% of the H_2O contribution is subtracted out of the $H_2O/C_{10}H_8 \approx 15$ spectrum. At some point, the differences in the H_2O band profile caused by the presence of the $C_{10}H_8$ negate the value of further subtraction. At this point the relative strength of the C—H stretches usually approach, but generally do not quite attain, that seen for pure naphthalene (values of about 4–6). Thus, within our usual uncertainties, we see no evidence that the presence of the H_2O causes a significant change in the overall strength of the C—H stretching mode; it simply "hides" it.

Thus, determination of the strength of the C—H stretching bands of $C_{10}H_8$ in H_2O is problematic, even when the matrix is well understood and the spectra of relevant laboratory standards are available. Making such corrections to astronomical data will be even more difficult given the uncertain crystalline state of the ice along the line of sight and the possible presence of multiple components or other species like CH_3OH and NH_3 that can alter the profile of the underlying H_2O band. As a rule, measurements are likely to *underestimate* the true C—H stretching mode absorption.

Despite the difficulty in measuring them, it is clear the C—H stretching features of $C_{10}H_8$ in H_2O ice are moderately shifted to higher frequencies than seen for pure $C_{10}H_8$ (Fig. 8, Tables 1 and 2). The C—H stretching bands show similar behavior to the

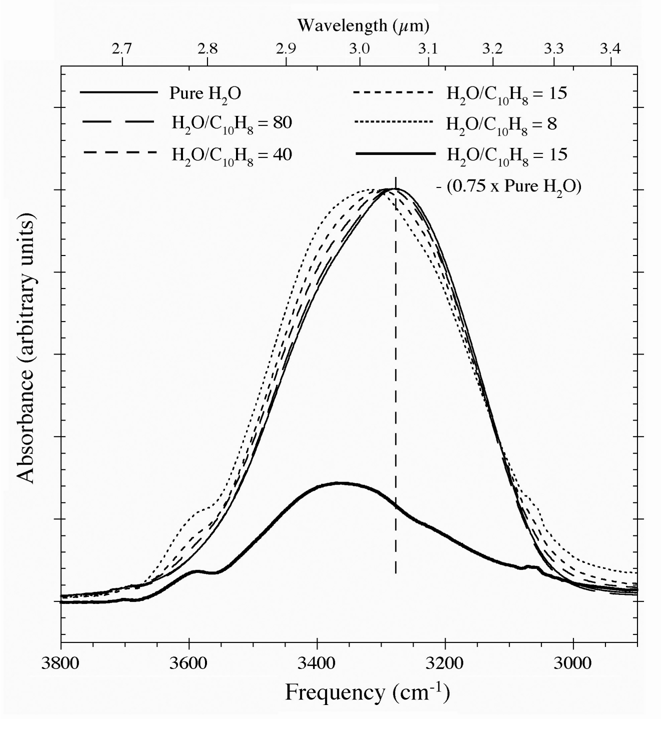

FIG. 9.—Profile of the O—H stretching feature of a pure H_2O ice and $H_2O—C_{10}H_8$ samples having various $C_{10}H_8$ concentrations at 15 K. Increasing concentrations of $C_{10}H_8$ cause the feature's centroid to move to higher frequencies, produce a dangling O—H feature near 3600 cm^{-1} (2.8 μm), and alters the low-frequency wing of the band. The lower trace shows the residuals that remain after 75% of the 3.0 μm H_2O feature is removed from the spectrum of the $H_2O—C_{10}H_8 \approx 15$ sample using the spectrum of the pure H_2O ice. Such corrections improve the apparent spectral contrast of the aromatic C—H stretching feature but cannot be taken to completion because of the $H_2O—C_{10}H_8$ interactions.

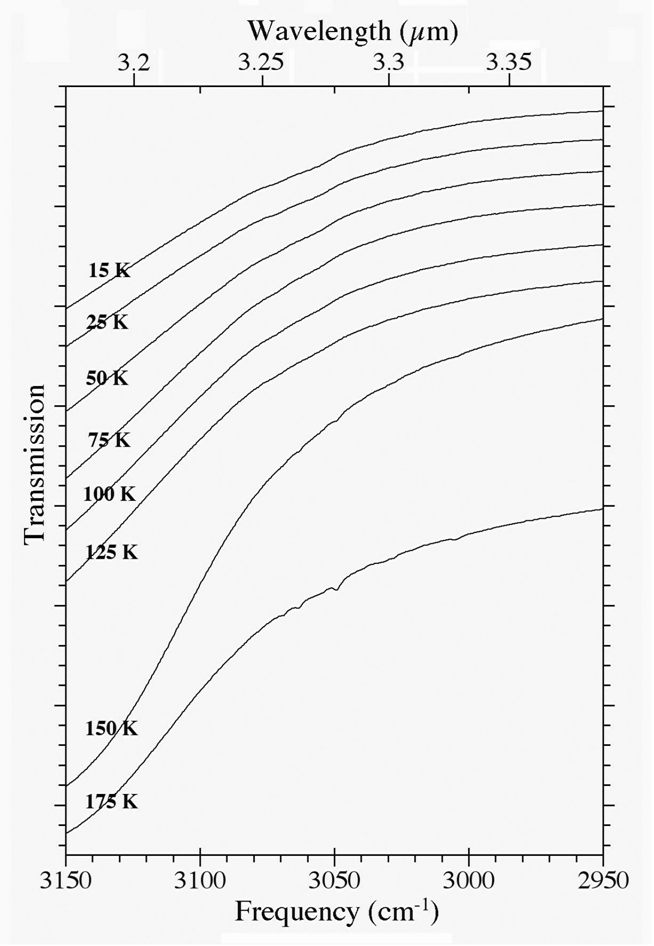

FIG. 10.—The 3150–2950 cm^{-1} (3.17–3.39 μm) spectra of an $H_2O/C_{10}H_8 \approx 15$ ice as a function of ice temperature. Spectra were taken from an ice deposited at 15 K that was subsequently warmed to 25, 50, 75, 100, 125, 150, and 175 K.

other $C_{10}H_8$ bands during warm up, namely the broadened bands seen at the lowest temperatures sharpen, shift, and split as the H_2O ice matrix crystallizes above 125 K (Fig. 10).

3.6. *The Absolute Band Strengths of Naphthalene in* H_2O *Ices*

The band strengths listed in Tables 1 and 2 are *relative* intensities; they are normalized to the area of the $C_{10}H_8$ band near 1390 cm^{-1}. Repeat experiments demonstrate that the relative areas of most bands are precise to better than 10% (typically better than 5%). The primary exceptions are (1) a few bands that overlap strong H_2O features, which makes it difficult to precisely determine spectral baselines (the aromatic C—H stretching feature and the 790 cm^{-1} CH out-of-plane bending feature), and (2) very weak bands detected with low signal-to-noise ratios. The variations between different spectra for these bands can be up to 50%. Thus, the relative strengths in Tables 1 and 2 are reasonably well-established values and can be used to assist with the identification of $C_{10}H_8$ in H_2O ices and predict the strengths of unobserved features on the basis of previously measured bands.

However, the use of band areas in laboratory or astronomical spectra to derive column densities requires *absolute* integrated band strengths. Provided that the concentration K is known, the most direct way to derive absolute band strengths is to scale against other bands in the spectrum whose strengths are known, in this case the bands of H_2O. The column densities of H_2O and $C_{10}H_8$ in our $H_2O/C_{10}H_8 = K$ samples are given by

$$N_{\mathrm{H_2O}} = \frac{\left(\int \tau\, d\nu\right)_{\mathrm{H_2O}}}{A_{\mathrm{H_2O}}},$$

$$N_{\mathrm{naph}} = \frac{N_{\mathrm{H_2O}}}{K} = \frac{\left(\int \tau\, d\nu\right)_{\mathrm{naph}}}{A_{\mathrm{naph}}}, \qquad (1)$$

where $N_{\mathrm{H_2O}}$ and N_{naph} are the column densities of H_2O and $C_{10}H_8$ in molecules cm^{-2}, $A_{\mathrm{H_2O}}$ and A_{naph} are the band strengths of the relevant features in cm $molecule^{-1}$, and $(\int \tau\, d\nu)_{\mathrm{H_2O}}$ and $(\int \tau\, d\nu)_{\mathrm{naph}}$ are the bands' areas in absorbance (in units of cm^{-1}). Combining the equations and solving for A_{naph} yields

$$A_{\mathrm{naph}} = K\left(\int \tau\, d\nu\right)_{\mathrm{naph}} \frac{A_{\mathrm{H_2O}}}{\left(\int \tau\, d\nu\right)_{\mathrm{H_2O}}}. \qquad (2)$$

The column density of H_2O was determined by measuring the band areas of the O—H stretching mode (3300 cm^{-1}; 3.0 μm) and H—O—H bending mode (1660 cm^{-1}; 6.0 μm) of H_2O ice and assuming band strengths of 1.7×10^{-16} and 1.0×10^{-17} cm $molecule^{-1}$, respectively (Hudgins et al. 1993). Using equation (2) to make multiple derivations of the strengths of the $C_{10}H_8$ bands near 1390, 1270, and 790 cm^{-1} (7.19, 7.87, and 12.7 μm) using both H_2O bands and the band areas obtained from our $H_2O/C_{10}H_8 = 8$, 15, and 40 samples yields values of $A_{1390} = (8.1 \pm 0.7) \times 10^{-19}$ cm $molecule^{-1}$, $A_{1270} = (4.2 \pm 0.9) \times 10^{-19}$ cm $molecule^{-1}$, and $A_{790} = (1.1 \pm 0.1) \times 10^{-17}$ cm $molecule^{-1}$. Thus, the *relative* strengths reported in Tables 1 and 2 can be converted to *absolute* strengths by multiplying all the values by a factor of 8.1×10^{-19} cm $molecule^{-1}$.

The absolute strengths of selected bands are listed in Table 3, where they are compared with values measured in Ar matrices and in pure $C_{10}H_8$ and the calculated band strengths of gas-phase $C_{10}H_8$. The Ar values are scaled to the calculated strength of the 1390 cm^{-1} band of gas-phase $C_{10}H_8$, and the pure $C_{10}H_8$ values are scaled to the strength of the same bands as measured for our H_2O—$C_{10}H_8$ samples. Experiments in which we used a HeNe laser to monitor sample thicknesses during deposition yielded estimates of absolute band strengths for pure $C_{10}H_8$ and $C_{10}H_8$ isolated in N_2 that are consistent with these scaled values to within our stated uncertainties.

The derived values of the 1390, 1270, and 790 cm^{-1} bands differ by factors of about 1.5, 0.3, and 0.6, respectively, from the strengths predicted from quantum mechanical calculations for gas-phase $C_{10}H_8$ (Langhoff 1996); i.e., they agree to within a factor of 2–3. When normalized to the 1390 cm^{-1} band, the band strengths of $C_{10}H_8$ in H_2O are found to agree to within 50% of the values observed in Ar matrices (Hudgins & Sandford 1998a). Such variations are comparable to the uncertainties in our $H_2O/C_{10}H_8$ sample ratios (§ 2). Thus, while *relative* band strengths do differ, indicating that *individual* band strengths can change (either increasing or decreasing) by up to factors of 2–3, there is no evidence within our uncertainties that the intrinsic strengths of the $C_{10}H_8$ absorptions are *systematically* strengthened or weakened by the presence of the H_2O matrix.

As described in § 3.5, the C—H stretching features represent a special problem for H_2O—$C_{10}H_8$ mixes because of the loss of spectral contrast of the features due to the underlying 3.0 μm H_2O feature. However, we find no evidence suggesting the

TABLE 3

ABSOLUTE STRENGTHS OF THE STRONGER NAPHTHALENE ABSORPTION BANDS

PURE NAPHTHALENE (15 K)		H_2O/NAPHTHALENE = 15 (15 K)		NAPHTHALENE IN ARGON (15 K)[a]		GAS-PHASE NAPHTHALENE (CALCULATED)[b]	
Band Position[c] (cm^{-1})	Intensity[d] ($\times 10^{-19}$ cm $molecule^{-1}$)	Band Position[c] (cm^{-1})	Intensity[e] ($\times 10^{-19}$ cm $molecule^{-1}$)	Band Position[c] (cm^{-1})	Intensity[f] ($\times 10^{-19}$ cm $molecule^{-1}$)	Band Position (cm^{-1})	Intensity ($\times 10^{-19}$ cm $molecule^{-1}$)
618.0	2.8	618.0	4.7	621.2, 619.3	3.1	632.1	5.3
783.4*	120	791.2	109	788.2, 783.4	84	788.4	185
962.2	4.7	968.3	2.8	957.6*	2.9	963.5	7.1
1010.6*	6.1	1010.7	5.4	1016.4, 1012.4	6.0	1009.7	6.8
1128.9*	5.2	1129.9	4.4	1129.1*	4.3	1131.9	5.3
1211.4	3.4	1212.2	2.6	1214.2*	1.6	1208.8	2.0
1243.6	2.4	1245.8	2.5	1237.1*	1.9		
1270.0	5.8	1270.9	4.9	1272.8*	5.9	1270.0	13.6
1390.2	*8.1*	1391.3	*8.1*	1391.8*	*5.3*	1399.8	*5.3*
1507.5, 1510.5	11.5	1510.7, 1506.9	12.7	1513.0*, 1498.9	6.4	1507.9	15.1
1462.1	0.6						
1596.7	5.3	1597.2	5.2	1604.4	4.9	1593.3	10.5
1733.6	3.2			1722.4	1.8		
1819.5	. . .			1806.3*	. . .		
1843.9	. . .						
1875–1795	4.2						
1914.0	7.4			1909.8*	. . .		
1953.1	. . .						
3051.3*	. . .	~3071	. . .	3065.0*	. . .	3062.5	131[h]
3114–2995[i]	50[i]	~3055	. . .	3078.2*	. . .	3076.5	118[h]
		3080–3040	(50)[g]	3117–2934[i]	55[i]		
				3087–3048[i]	38[i]		

[a] Ar matrix data are taken from Hudgins & Sandford 1998a.

[b] Calculated values from Langhoff 1996.

[c] An asterisk signifies that the value is the position of the strongest band(s) or an associated group of bands. Only the strongest of the C—H stretching bands are listed.

[d] Absolute strengths are based on the assignment of a value of 8.1×10^{-19} cm $molecule^{-1}$ for the strength of the band near 1390 cm^{-1}, the value measured for $C_{10}H_8$ in H_2O in this work.

[e] Absolute strengths are based on the assignment of a value of 8.1×10^{-19} cm $molecule^{-1}$ for the strength of the band near 1390 cm^{-1} and the use of the relative band strengths of our $H_2O/C_{10}H_8 \approx 15$ sample (see § 3.6).

[f] Absolute strengths are based on the assignment of a value of 5.3×10^{-19} cm $molecule^{-1}$ for the strength of the band near 1390 cm^{-1}, the value calculated for this band by Langhoff 1996.

[g] Assumes the same relative and absolute strengths of pure $C_{10}H_8$ (see §§ 3.5 and 3.6).

[h] Calculated values for the C—H stretch in PAHs are generally about a factor of 2 too strong (see Hudgins & Sandford 1998a).

[i] Relative band area of all the C—H stretching bands within the stated frequency range.

intrinsic strength of the aromatic C—H stretch of $C_{10}H_8$ in H_2O is substantially different from that of pure $C_{10}H_8$, both because the relative strengths of these features were observed to approach those of pure $C_{10}H_8$ as progressively more of the underlying H_2O contribution was subtracted out and because the relative/intrinsic strengths of other bands are generally very similar. Thus, in Table 3 we have assumed the same relative strength for the C—H stretching bands in both pure $C_{10}H_8$ and $H_2O—C_{10}H_8$.

In summary, the H_2O induces modest changes in the intrinsic strengths of the various $C_{10}H_8$ bands. These can be either upward or downward, depending on the feature. *Overall, there is little systematic increase or decrease in the band strengths (perhaps none)*. These results indicate that one should be able to use calculated gas-phase PAH band strengths (i.e., Langhoff 1996; Bauschlicher & Langhoff 1997) to derive column densities from individual astronomical features and be accurate to within factors of 2–3, depending on the band. The measurement of multiple bands and/or the availability of relevant laboratory data would decrease this uncertainty.

4. ASTROPHYSICAL IMPLICATIONS

The laboratory results presented here have a number of implications for the detection and identification of PAHs in absorption in interstellar dense molecular clouds and H_2O-rich planetary ices and for the determination of their relative and absolute abundances.

4.1. *Detection of PAHs in Astrophysical Ices*

Solid-state interactions generally change spectral band positions, widths, and strengths from those of their gas-phase counterparts. However, in the case of naphthalene, these effects are relatively modest: peak position shifts relative to gas-phase or matrix-isolated values are less than 10 cm^{-1}, band widths increase by factors of 3–10, and individual relative band strengths vary by at most a factor of about 3. Overall, the intrinsic band strengths appear to be comparable to those of gas-phase and Ar-isolated $C_{10}H_8$. Thus, to first order the current database of band positions and strengths of gas-phase PAHs and PAHs in Ar matrices can be used for the search for absorption features of PAHs in dense clouds. The absorption bands of PAHs in H_2O will generally be 3–10 times wider than those in the Ar-isolated PAH database (Hudgins & Sandford 1998a, 1998b, 1998c). Nevertheless, final analysis of PAH absorption bands in dense cloud spectra will require laboratory studies of relevant H_2O-PAH ice mixtures to verify that the observed band positions, widths, and relative strengths are self-consistent. Relevant laboratory data will also be required if the column densities of the PAHs are to be determined to better than factors of 2–3. We are currently studying the IR spectra of additional PAHs in H_2O ices to further explore the extent of these variations.

The detection of interstellar PAHs on the basis of their absorption spectra will differ in several important ways from similar studies of PAHs in emission. First, the relative strengths of the various PAH absorption features will be *very* different from the PAH emission bands seen in other environments, environments where contributions from PAH ions, effects associated with the excitation/emission processes, etc., must be accounted for. Second, while the aromatic C—H stretching bands near 3030 cm^{-1} (3.3 μm) represent one of the most characteristic aromatic modes in emission spectra, their value in the absorption spectra of dense clouds is mitigated by their very poor spectral contrast in H_2O-rich ices.

4.2. *Determination of the Physical State of PAHs in Dense Clouds*

Dense molecular clouds have low radiation fields, low temperatures, and high densities relative to the diffuse interstellar medium. Under these conditions, PAHs are more likely to be seen in absorption than in emission. It is clear from § 3.1 that given adequate spectral resolution and signal-to-noise ratios, it is possible to distinguish the physical state of PAHs detected in absorption in dense clouds. PAHs in the gas phase will produce rovibrational envelopes with each vibrational mode showing the *P*, *Q*, and *R* branches characteristic of rotating gas-phase molecules (Cané et al. 1996; Figs. 2 and 3). Such spectral profiles are not only diagnostic of gas-phase PAHs, but the widths of the *P* and *R* branches will provide a measure of their rotational temperature. (Note that PAHs in interstellar clouds, being much colder, would be expected to show considerably narrower *P* and *R* envelopes than those shown in the laboratory spectrum in Fig. 3.)

In contrast, aromatics in the solid state will not show rovibrational spectral structure. Instead of multiple branches, solid-state PAHs will produce single features whose positions, widths, and relative strengths will depend on the nature of the matrix in which the PAH is frozen. PAHs frozen in inert matrices (such as solid N_2) will generally produce narrow bands, with many features showing several components associated with different matrix sites. The spectrum of $C_{10}H_8$ in an argon matrix (Figs. 1–3) serves as an example. PAHs in matrices that produce strong interactions will generally produce broad bands. The absorption bands produced by pure $C_{10}H_8$ and $C_{10}H_8$ in H_2O are both quite distinct from those of gas-phase $C_{10}H_8$ and $C_{10}H_8$ in an inert matrix. There are distinctive spectral differences between pure $C_{10}H_8$ and $C_{10}H_8$ in H_2O, but they are subtle. The two produce slightly different patterns of relative band strengths, and the bands of pure $C_{10}H_8$ generally fall systematically a few cm^{-1} to the red of the bands of $C_{10}H_8$ in H_2O.

Thus, using IR spectroscopy it should be possible to search for interstellar PAHs and determine whether they are in the gas phase, inert matrices, or more strongly interacting matrices. If appropriate laboratory data are available, it is also possible to place constraints on the composition of the matrix and, in some cases, the temperature of the matrix (§ 3). It should be noted, however, that distinguishing between these states will be considerably more complicated if the same lines of sight contain macromolecular materials that contain significant amounts of aromatic structures.

4.3. *Determination of PAH Identities and Abundances*

This work makes it clear that different matrices cause different changes in the positions, widths, and strengths of the absorption bands of naphthalene. Preliminary work done by us on a number of other H_2O-PAH mixtures indicates that although peaks are broadened and slightly shifted, the spectra of PAHs in H_2O generally closely resemble their published argon matrix spectra. This implies that armed with the current database of spectra from Ar matrix–isolated PAHs (see footnote 4 above), it should be possible to tentatively identify specific subclasses of PAHs in interstellar dense clouds on the basis of observed absorption band positions.

Using the absolute band strengths calculated for gas-phase PAHs, it should also be possible to estimate column densities of PAHs in absorption to within a factor of 3. Determination of more accurate column densities is problematic, however, and will require three things. First, since intermolecular interactions can cause significant relative and absolute changes in PAH band strengths, the composition of the matrix surrounding the PAH must be constrained by detection/identification of ice absorption features in the same spectra. Second, additional laboratory studies of the relevant PAHs in appropriate matrices may be required. Third, determination of column densities from multiple absorption bands is strongly recommended because relative peak-to-peak strength variations of factors of 2–3 are possible (§ 3.6).

The various PAH bands have different advantages and disadvantages for probing and identifying PAH families and for the determination of column densities. The C—H stretching features near 3.3 μm have the disadvantage of *very* poor spectral contrast due to the overlapping O—H stretch of H_2O (see § 3.5). In general, measurements of the band areas of these features are likely to represent *underestimates,* even when attempts are made to correct for underlying absorption due to H_2O or other species. These modes have the advantage, however, that they fall at nearly the same frequency for all PAHs, independent of size or structure. As a result, the amount of C—H stretching absorption can provide an assessment of the abundance of the *total* PAH population along a line of sight; i.e., it can provide a measure of the lower limit of cosmic carbon tied up in PAHs in dense clouds. It will not, however, be useful for the identification of specific aromatics. In contrast, the longer wavelength bands associated with C—C modes and C—H bending modes are more sensitive to molecular structure and therefore provide better diagnostic information for identifying individual species and classes of species, but these will provide less comprehensive information about the abundance of the total aromatic population. Thus, in principle, the identification of the aromatics in dense clouds waits largely on the acquisition of relevant, high-quality 3–20 μm IR spectra of dense clouds and additional laboratory spectra of PAH-ice mixtures.

4.4. *Implications for Previous Reports of PAH Absorption Bands in Dense Clouds*

Currently, there are only a few tentative reports of potential PAH absorption bands in the spectra of dense clouds. These include potential detections of aromatic C—H stretching mode bands near 3080 cm^{-1} (3.25 μm) (Sellgren et al. 1995; Brooke et al. 1999; Bregman & Temi 2001), an aromatic C—C stretch near 1610 cm^{-1} (6.21 μm) (Chiar et al. 2000), and a PAH out-of-plane bending mode band near 890 cm^{-1} (11.2 μm) (Bregman et al. 2000). Table 4 summarizes the implied column densities of aromatic C—H toward these various objects, along with their associated H_2O ice column densities and the resulting ratios of H_2O to aromatic C—H groups. The implied H_2O/PAH ratios depend on the size of the PAHs responsible. Subsequent columns in Table 4 provide the H_2O/PAH ratios that would result if all the PAHs had 8, 12, or 18 C—H groups per molecule. These values correspond to the condensed PAHs ranging in size from naphthalene ($C_{10}H_8$) up to the largest PAHs studied in Ar matrices to date. Of course, interstellar PAHs must span a wide distribution of species; the population of PAHs responsible for the ubiquitous emission features is thought to be dominated by species containing on the order of 80 C atoms.

It is apparent from Table 4 that the PAH concentrations implied by the astronomical data are modest, falling in the $H_2O/PAH = 20–100$ range, i.e., at values of a few percent. These values are most comparable to our $H_2O/C_{10}H_8 \approx 40$ samples. These values are consistent with the overall muted appearance of the C—H absorption bands in the astronomical data. Furthermore, the $H_2O/C_{10}H_8 \approx 40$ spectra suggest that many other aromatic absorption bands should be observable in the spectra of these objects, although high-quality spectra will be required for their detection.

4.5. *Implications for PAHs in Solar System Ices*

Numerous bodies in the outer solar system appear to contain both H_2O-rich ices and dark organic materials. The nature of the organic materials is poorly understood, but the presence of aromatic species is a strong possibility. While the laboratory work presented here has focused on the implications for interstellar ices, it may also be of value to the interpretation of future spectral data from icy bodies in the solar system. In this regard, the spectra taken at higher temperatures may be of particular interest.

5. CONCLUSIONS

Polycyclic aromatic hydrocarbons are observed in emission in a wide variety of astrophysical environments and represent one of the most ubiquitous classes of molecules in space. In most environments the PAHs are detectable via their characteristic IR emission features, but PAHs in dense clouds are expected to be seen in absorption. While they could be present as cold gas, most PAHs in dense clouds are expected to reside in ice mantles surrounding dust grains.

Our laboratory results demonstrate that the positions, widths, and strengths of the absorption bands of the PAH

TABLE 4

THE CONCENTRATION OF PAHs IN INTERSTELLAR H_2O ICES

Object	H_2O (molecules cm^{-2})	Aromatic C—H (groups cm^{-2})	H_2O/Aromatic C—H	$H_2O/C_{10}H_8$	$H_2O/C_{24}H_{12}$	$H_2O/C_{54}H_{18}$
Mon R2/IRS 3	5.9×10^{18}[a]	1.8×10^{18}[b]	3.3	26	40	59
GL 2591	1.6×10^{18}[c]	4.1×10^{17}[d]	3.9	31	47	70
S140	5.6×10^{18}[a]	9.4×10^{17}[d]	6.0	48	72	108
GL 989	4.6×10^{18}[a]	1.2×10^{18}[d]	3.8	30	46	68
Elias 29	6.0×10^{18}[a]	2.1×10^{18}[d]	2.9	23	35	47

[a] From band areas of the 6.0 μm H_2O ice band (Keane et al. 2001).

[b] Sellgren et al. 1995.

[c] Estimated from the optical depth of the 6.0 μm band H_2O ice band reported by Willner et al. 1982.

[d] Bregman & Temi 2001.

naphthalene are altered from the gas phase when placed in a solid matrix. Gas-phase $C_{10}H_8$ shows the characteristic *P, Q,* and *R* branches of the rovibrational transitions of gas-phase molecules. However, these rovibrational features are replaced by purely vibrational features when $C_{10}H_8$ is condensed. The IR spectrum of solid $C_{10}H_8$ varies depending on the nature of the interaction with the surrounding matrix material. If the matrix is relatively inert, like argon or N_2, the $C_{10}H_8$ features are narrow (generally FWHM < 2 cm^{-1}) and may show multiple components associated with different matrix sites. In more interactive matrices, like pure solid $C_{10}H_8$ and $C_{10}H_8$ in H_2O, the $C_{10}H_8$ bands are 3–10 times broader, show variable band position shifts (0–10 cm^{-1} in either direction), and show variable changes in *relative* band strengths (typically factors of 1–3). However, there is no evidence for a systematic increase or decrease in the intrinsic *absolute* band strengths compared to isolated naphthalene. Perhaps the most dramatic difference in H_2O matrices is the large loss of spectral contrast of the C—H stretching feature near 3.3 μm.

These matrix-dependent changes make it fairly easy to distinguish between the presence of cold gas phase PAHs, PAHs in inert matrices, and PAHs in strongly interacting matrices. If appropriate laboratory data are available, it is also possible to place some constraints on the composition of the matrix. Interpretation of the aromatic features will be more complicated, however, if aromatic-containing macromolecular materials are also present in the clouds.

The band positions, widths, and relative strengths of the IR bands of $C_{10}H_8$ in pure form and in H_2O-rich ices are similar but show characteristic differences. In H_2O ices, the $C_{10}H_8$ bands are relatively insensitive to concentration and temperature, with the exception that all the bands show dramatic changes when warmed above 125 K, where amorphous H_2O ice converts to its cubic and hexagonal crystalline forms. Of the various $C_{10}H_8$ peaks, those near 1597, 1510, 1270, 1130, 1011, 968, and 790 cm^{-1} are the most sensitive to matrix interactions.

Taken *in toto,* these results indicate that it should be possible to use the current database of spectra from Ar matrix–isolated PAHs to tentatively identify specific PAHs or subclasses of PAHs in interstellar dense clouds on the basis of observed absorption band positions. Better identifications could be made using appropriate laboratory ice-PAH spectra for comparison. It should also be possible to calculate relevant column densities that are accurate to better than a factor of 3 for any PAHs identified in absorption in dense clouds. Determination of the column densities of aromatics to better than a factor of 3 will, however, require good knowledge about the nature of the matrix in which the PAH is embedded and information from laboratory studies of relevant samples.

The limited number of tentative identifications of PAH absorption bands in dense clouds suggest that the PAHs are present at concentrations of a few percent. These concentrations are consistent with the appearance of laboratory samples having similar concentrations.

The authors wish to express their sincere thanks to E. Cané, who kindly provided us with the gas-phase naphthalene spectra shown in Figures 1, 2, and 3. This work was fully supported by NASA's Laboratory Astrophysics (grant 188-02-04-02), Long Term Space Astrophysics (grant 188-44-57-01), Origins of Solar Systems (grant 344-37-44-01), Exobiology (grant 344-38-12-04), Astrobiology (grant 344-50-92-02), and Planetary Geology and Geophysics (grant 344-30-21-01) programs. We gratefully acknowledge the expert technical and experimental support of Robert Walker. This paper benefited from the comments of an anonymous referee.

REFERENCES

Allamandola, L. J., Hudgins, D. M., & Sandford, S. A. 1999, ApJ, 511, L115

Allamandola, L. J., & Sandford, S. A. 1988, in Dust in the Universe, ed. M. E. Bailey & D. A. Williams (Cambridge: Cambridge Univ. Press), 229

Allamandola, L. J., Tielens, A. G. G. M., & Barker, J. R. 1989, ApJS, 71, 733

Bauschlicher, C. W., Jr., & Langhoff, S. R. 1997, Spectrochim. Acta A, 53, 1225

Behringer, R. E. 1958, J. Chem. Phys., 29, 537

Bernstein, M. P., Dworkin, J., Sandford, S. A., & Allamandola, L. J. 2001, Meteoritics Planet. Sci., 36, 351

Bernstein, M. P., Elsila, J. E., Dworkin, J. P., Sandford, S. A., Allamandola, L. J., & Zare, R. N. 2002, ApJ, 576, 1115

Bernstein, M. P., Moore, M. H., Elsila, J. E., Sandford, S. A., Allamandola, L. J., & Zare, R. N. 2003, ApJ, 582, L25

Bernstein, M. P., Sandford, S. A., Allamandola, L. J., Chang, S., & Scharberg, M. A. 1995, ApJ, 454, 327

Bernstein, M. P., Sandford, S. A., Allamandola, L. J., Gillette, J. S., Clemett, S. J., & Zare, R. N. 1999, Science, 283, 1135

Blake, D., Allamandola, L., Sandford, S., Hudgins, D., & Freund, F. 1991, Science, 254, 548

Bregman, J. D., Hayward, T. L., & Sloan, G. C. 2000, ApJ, 544, L75

Bregman, J. D., & Temi, P. 2001, ApJ, 554, 126

Brooke, T. Y., Sellgren, K., & Geballe, T. R. 1999, ApJ, 517, 883

Cané, E., Palmieri, P., Tarroni, R., Trombetti, A., & Handy, N. C. 1996, Gazz. Chim. Italiana, 126, 289

Chiar, J. E., Tielens, A. G. G. M., Whittet, D. C. B., Schutte, W. A., Boogert, A. C. A., Lutz, D., van Dishoeck, E. F., & Bernstein, M. P. 2000, ApJ, 537, 749

Dartois, E., Schutte, W., Geballe, T. R., Demyk, K., Ehrenfreund, P., & d'Hendecourt, L. 1999, A&A, 342, L32

Ehrenfreund, P., & Charnley, S. B. 2000, ARA&A, 38, 427

Ehrenfreund, P., Dartois, E., Demyk, K., & d'Hendecourt, L. 1998, A&A, 339, L17

Gerakines, P. A., et al. 1999, ApJ, 522, 357

Hudgins, D. M., & Allamandola, L. J. 1995a, J. Phys. Chem. A, 99, 3033

———. 1995b, J. Phys. Chem. A, 99, 8978

Hudgins, D. M., & Sandford, S. A. 1998a, J. Phys. Chem. A, 102, 329

———. 1998b, J. Phys. Chem. A, 102, 344

———. 1998c, J. Phys. Chem. A, 102, 353

Hudgins, D. M., Sandford, S. A., & Allamandola, L. J. 1994, J. Phys. Chem. A, 98, 4243

Hudgins, D. M., Sandford, S. A., Allamandola, L. J., & Tielens, A. G. G. M. 1993, ApJS, 86, 713

Jenniskens, P., & Blake, D. F. 1994, Science, 265, 753

Jenniskens, P., Blake, D. F., Wilson, M. A., & Pohorille, A. 1995, ApJ, 455, 389

Keane, J. V., Tielens, A. G. G. M., Boogert, A. C. A., Schutte, W. A., & Whittet, D. C. B. 2001, A&A, 376, 254

Langhoff, S. R. 1996, J. Phys. Chem., 100, 2819

Peeters, E., Hony, S., van Kerckhoven, C., Tielens, A. G. G. M., Allamandola, L. J., Hudgins, D. M., & Bauschlicher, C. W. 2002, A&A, 390, 1089

Sandford, S. A. 1996, Meteoritics Planet. Sci., 31, 449

———. 2002, Planet. Space Sci., 50, 1145

Sandford, S. A., & Allamandola, L. J. 1990, ApJ, 355, 357

———. 1993, ApJ, 417, 815

Sandford, S. A., Allamandola, L. J., Tielens, A. G. G. M., & Valero, G. J. 1988, ApJ, 329, 498

Sellgren, K., Brooke, T. Y., Smith, R. G., & Geballe, T. R. 1995, ApJ, 449, L69

Smith, R. G., Sellgren, K., & Tokunaga, A. T. 1989, ApJ, 344, 413

Szczepanski, J., Wehlburg, C., & Vala, M. 1995, Chem. Phys. Lett., 232, 221

Willner, S. P., et al. 1982, ApJ, 253, 174

Witteborn, F. C., Sandford, S. A., Bregman, J. D., Allamandola, L. J., Cohen, M., & Wooden, D. 1989, ApJ, 341, 270